Edge dislocations in multicomponent solid solution alloys: Beyond traditional elastic depinning

A. Esfandiarpour [1], S. Papanikolaou [1], and M. Alava[1,2]

[1]*NOMATEN Centre of Excellence, National Centre for Nuclear Research, ul. A. Soltana 7, 05-400 Swierk/Otwock, Poland*
[2]*Department of Applied Physics, Aalto University, PO Box 11000, 00076 Aalto, Finland*

High-entropy alloys (HEA) form solid solutions with large chemical disorder and excellent mechanical properties. We investigate the origin of HEA strengthening in face-centered-cubic (fcc) single-phase HEAs through molecular dynamics simulations of dislocations, in particular, the equiatomic CrCoNi, CrMnCoNi, CrFeCoNi, CrMnFeCoNi, FeNi, and, also, $Fe_{0.4}Mn_{0.27}Ni_{0.26}Co_{0.05}Cr_{0.02}$, $Fe_{0.7}Ni_{0.11}Cr_{0.19}$. The dislocation correlation length ξ, roughness amplitude R_a, and stacking fault widths W_{SF} are tracked as a function of stress. All alloys are characterized by a well defined depinning stress (σ_c) and we find a regime where exceptional strength is observed, and a fortuitous combination takes place, of small stacking fault widths and large dislocation roughness R_a. Thus the depinning of two partials seems analogous to unconventional domain wall depinning in disordered magnetic thin films. This regime is identified in specific compositions commonly associated with exceptional mechanical properties (CrCoNi, CrMnCoNi, CrFeCoNi, and CrMnFeCoNi). Yield stress from analytical solute-strengthening models underestimates largely the results in these cases. A possible strategy for increasing strength in multicomponent single-phase alloys is the combined design of stacking fault width and element-based chemical disorder. A hardening factor represents this strategy where combination of low stacking fault and high misfit parameters (and thus high roughness of dislocation at depinning stress) leads to stronger fcc multicomponent alloys.

Solid solution strengthening is one of the key strategies to increase the yield stress of crystalline alloys by introducing solutes that pin dislocations through disturbances in the perfect lattice. In an extreme limit of this process, high entropy alloys (HEAs) are composed of four or more nearly equimolar alloying elements and they display single-phase behavior with outstanding mechanical properties [1–4]. Despite athermal transformation processes such as twining [3], crystal plasticity in HEAs is as common as in any crystal [5], mainly driven by dislocation dynamics, but with two key additional variables: chemical-induced-disorder lattice misfit and stacking fault width fluctuations. Common analytical models for solid solution strengthening in HEAs have been focused on quantifying the misfit contributions. For traditional alloys, strengthening was modeled by Fleischer [6] and Labusch [7]. They utilized the interaction between solute atoms and the pressure field of a dislocation as the core to their models. In these models, interactions related to the atomic size and shear modulus misfits play an important role in that the larger the difference between solute and solvent atom sizes, the stronger the pinning of dislocations. Beyond traditional solid solution alloys (SSA), in HEAs, a mean-field atomistic potential by Varvenne *et al.* [1,8] was used to identify an effective medium

alloy as a reference for HEA with the same average mechanical properties. In this way, Varvenne *et al.* calculated the interaction energy between solutes and dislocations and provided a scaling relationship between strengthening and misfit parameters. Although some studies addressed the relation between stacking fault energy and mechanical properties [9–11], the complexity of stacking fault fluctuations has been left unexplored. In a recent study [12], Zaiser *et al.* addressed the metastability and flow stress of partial dislocations based on the distance between two partial dislocations. In order to investigate the possible effects of stacking fault fluctuations, we study the mechanical properties of edge dislocations and their mobility under externally applied stress for seven fcc SSAs. We find that, for the top four stronger alloys, mechanical strength is controlled by a fortuitous combination of small stacking fault widths and chemical-disorder-induced large dislocation roughness, causing dislocation partials' overhangs, possibly analogous to unconventional depinning behaviors in disordered magnetic thin films.

Traditional elastic depinning theory [13,14] has been long thought to be the core basis of the description of the behavior of single dislocations in general disordered environments [14–16], and more specifically in solid solutions [17,18], where chemical disorder proliferates. The key prediction of such elastic depinning theories is the onset of a characteristic length scale, the dislocation correlation length ξ, below which the dislocation line displays fractal characteristics with nontrivial roughness. The length ξ is further predicted to scale with the applied stress in a power law manner, maximize at yielding (the depinning transition point), and

---

depend mainly on the dislocation line tension and the disorder fields' fluctuation features. Furthermore, in such theories, the yield point is controlled by the disorder fields' maximum strength, analogous to typical solid solution strengthening theories [1–4]. Nevertheless, traditional elastic depinning theory does not address the added complexity of the dislocation stacking fault, namely the fact that a gliding dislocation is composed of two dislocation partials' lines that glide together and are separated by a high-energy stacking fault, of average width W_{SF}. In metallurgy of pure single-component metals, the width W_{SF} is inversely correlated to the material's yield strength [19], but its role in strengthening of multicomponent metals, when strong disorder is also present, has been unexplored.

We investigate the interplay of disorder and stacking faults, by investigating a multitude of equiatomic solid solutions through the use of molecular dynamics simulations [20]. The choices of the studied materials are motivated by prior studies that provided benchmarks for traditional depinning behavior ($Fe_{0.7}Ni_{0.11}Cr_{0.19}$ [17] and FeNi [18]), and also by motivating experimental findings on equiatomic multicomponent alloys (CrCoNi, CrMnCoNi, CrFeCoNi, CrMnFeCoNi, and $Fe_{0.4}Mn_{0.27}Ni_{0.26}Co_{0.05}Cr_{0.02}$) that point towards exceptional strength [21–25]. Equiatomic fcc HEAs with low stacking fault energy showed an excellent balance between strength and ductility, particularly at cryogenic temperatures [3,4]. In an experimental study [4], it was shown that the yield strength of the alloys has the following order at 77 K: CrCoNi > CrMnCoNi > CrFeCoNi > CrMnFeCoNi, which indicates that the alloys with the most elements are not necessarily the strongest. Using molecular dynamics (MD) simulations, this Letter focuses on the mobility and geometry of edge dislocations in several random HEAs, employing LAMMPS [26] and modified embedded atom method (MEAM) interatomic potential [27]. Our focus is the depinning behavior of a model configuration of single edge dislocations under shear stress that drive ideal dislocation glide at the low temperature of 5 K.

MD simulations can successfully describe the complicated interaction between stacking faults and chemical disorder during loading, at the atomic scale [17,18]. There are several MD based studies that explained the core structure of dislocations as well as the interaction of dislocations with solutes in fcc traditional alloys [17,18,28]. Consistent with these prior studies, our simulations are characterized by a simulation cell with fcc crystal and random distribution of constituent elements, created along $X = [110](l_x = 252\ \text{Å})$, $Y = [\bar{1}11](l_y = 122\ \text{Å})$, and $Z = [1\bar{1}2](l_z = 2002\ \text{Å})$ containing 5 432 700 atoms [see Fig. 1(a)]. A periodic array of dislocations (PAD) model [29] was used to insert perfect $\frac{1}{2}\langle 110 \rangle$ edge dislocation between the two central [111] planes in the cell. Periodic boundary conditions (PBC) are applied in both X and Z direction, while the fixed boundary condition is used in the Y direction. Volume along the Y direction is divided into three regions, where the central region contains the usual MD mobile atoms and is sandwiched between the fixed upper and lower regions of several atomic layers. First, atomic relaxation is performed using the NPT ensemble to ensure that the stresses in X and Z directions are minimized. Then stress-controlled loading is considered where the force $F_x = \sigma A N_{\pm} e_{xz}$ is applied to the upper $(+)$ and lower regions $(-)$ with the area of A and $N\pm$
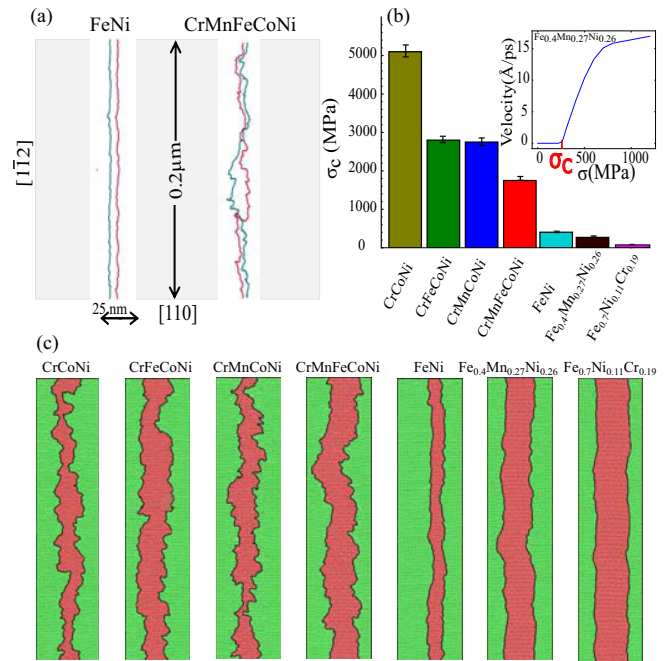

FIG. 1. (a) Two partial dislocation lines dissociated from an edge dislocation for equimolar FeNi and CrMnFeCoNi alloys during flow. Dislocation line direction [1 − 12] and Burgers vector direction [110] as well as the size of the box in these directions are presented. (b) σ_c for all the alloys in this study. The inset represents the dislocation velocity as a function of σ for $Fe_{0.4}Mn_{0.27}Ni_{0.26}Co_{0.05}Cr_{0.02}$, and beyond $\sigma \geqslant \sigma_c$ the dislocation keeps moving. (c) Two partial dislocations separated by stacking fault (red) at depinning stress for seven SSAs. Atoms with fcc and hcp structures are colored by green and red, respectively.

atoms. The simulations are performed in the NVE ensemble with the temperature controlled by a Berendsen thermostat at 5 K [30]. A time step of 4 fs is used. All seven elemental compositions are simulated up to 300–600 MPa above depinning stress (10–20 different stress values). Each alloy composition is realized three different times. Dislocation and crystal structures are analyzed using a dislocation extraction algorithm (DXA) [31] and common neighbor analysis that are implemented in OVITO software [32]. Beyond the apparent computational intensity of this work, it is worth mentioning that the results of this work are based on the analysis of more than 0.5 PB of atomic configurational data that is locally stored, given that the dynamics of dislocations is tracked for 10–20 loading stresses at many time steps (120) for every alloy.

The characteristics of the geometry and mobility of edge dislocations in different HEAs are shown in Fig. 1 and Fig. 2. Figure 1(a) has a dislocation line direction [1 − 12] and Burgers vector direction along [110]. The figure shows two Shockley partial dislocations in their glide plane, which are dissociated from an edge dislocation for equimolar FeNi and CrMnFeCoNi alloys when σ has a large value of 2000 MPa. The overhang of partial dislocations in CrMnFeCoNi can be seen in this figure. Figure 1(b) shows the depinning stress (σ_c) identified for seven HEAs. σ_c is the stress at which the dislocation keeps moving [see the inset of Fig. 1(b)]. Based
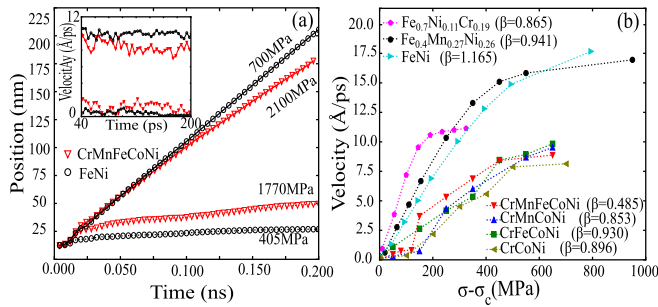
FIG. 2. (a) Position and velocity of an edge dislocation as a function of time for equimolar FeNi and CrMnFeCoNi for two different applied stress values. (b) The velocity of edge dislocation as a function of applied shear stress subtracted by depinning stress (σ_c) for several SSAs. β was calculated by fitting these data with a power-law form [14].

on σ_c, we identify two classes of alloys—the four stronger (i.e., CrCoNi, CrMnCoNi, CrFeCoNi, and CrMnFeCoNi) and the three softer ones (i.e., FeNi, $Fe_{0.4}Mn_{0.27}Ni_{0.26}Co_{0.05}Cr_{0.02}$, and $Fe_{0.7}Ni_{0.11}Cr_{0.19}$). Figure 1(c) shows the stacking fault area and roughness for all these alloys at their corresponding depinning stress. While all alloys host rough dislocations, the roughness of the four stronger alloys displays overhangs that resemble domain walls in disordered ferromagnetic thin films [33–35] that lead to dipolar-forces dominated crossover effects [35]. It is also worth noting that the observed alloy CrCoNi with the largest depinning stress and visibly large roughness has the smallest stacking fault area, consistent with experimental evidence on the key role of stacking faults for this alloy [22].

The roughness of a dislocation line is given by [17,18] $R(l) = \langle [x(z+l) - x(z)]^2 \rangle^{\frac{1}{2}}$, where x and z represent glide and dislocation line directions, respectively [Fig. 1(a)] and $x(z)$ refers to the dislocation segment position at height z. As $(\sigma \rightarrow \sigma_c)$, dislocations relax to new configurations through avalanches [14]. For $\sigma < \sigma_c$, one defines also the Hurst exponent H through [17,18,36]: $\ln(R) = H \ln(l) + c$, with H ranging in [0.5–1] for dislocation lines [17,18,36]. Going beyond σ_c, the mobility of dislocations is influenced by dislocation-solute interactions. In fcc SSAs, the relationship between the velocity of dislocation line and external stress is [14,17,28] $v(\sigma) \propto (\sigma - \sigma_c)^\beta$. Figure 2(a) shows first the position and the velocity of an edge dislocation as a function of time for equimolar FeNi and CrMnFeCoNi in two different σ. Figure 2(b) represents velocity as a function of $\sigma - \sigma_c$, which is then fitted accordingly. The variation of the exponent values β is unexpected and we interpret it as a result of strong collective pinning of the two partials; indeed, recently similar physics has been found in magnetic domain walls underlining the importance of collective phenomena [37]. It is clear that the effective β exponent is higher for the three softer alloys than for the other four alloys and, meanwhile, FeNi and $Fe_{0.7}Ni_{0.11}Cr_{0.19}$ show similar results to previous studies [17,28].

Figure 3(a) represents the radial distribution function [$g(r)$] for CrCoNi and CrMnFeCoNi alloys when $\sigma = \sigma_c$. More fluctuations in $g(r)$ can be seen for the strongest alloy (i.e.,
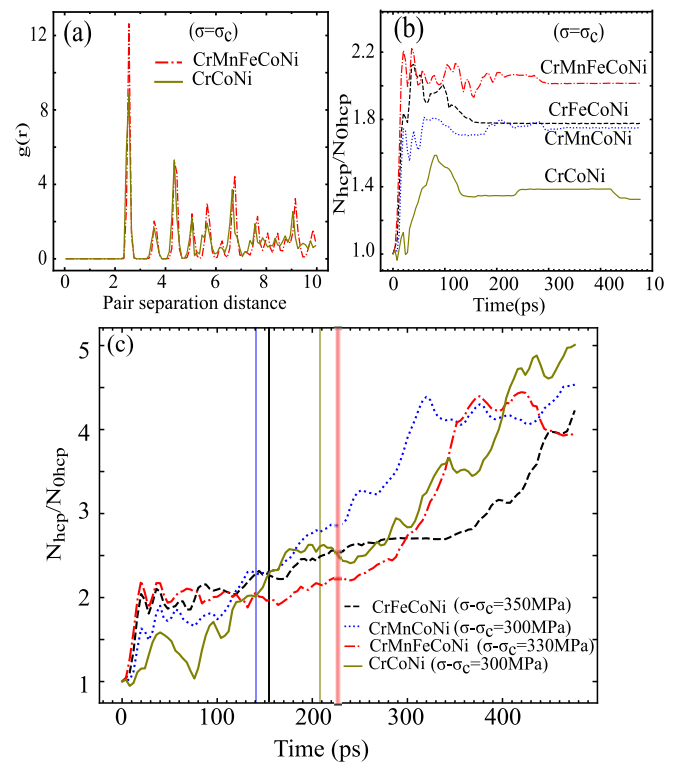

FIG. 3. (a) Radial distribution function [$g(r)$] for CrCoNi and CrMnFeCoNi alloys when $\sigma = \sigma_c$. The ratio of N_{hcp}/N_{0hcp} as function of time, where N_{0hcp} is the number of hcp atoms at $t = 0$ between two partial dislocation lines for the four stronger alloys when (b) $\sigma = \sigma_c$ and (c) $\sigma > \sigma_c + 300$ MPa. The straight lines separate two different regimes for each alloy.

CrCoNi). While, at $\sigma \leqslant \sigma_c$, the number of hexagonal close packed (hcp) atoms inside the stacking faults approaches a constant value [Fig. 3(b)], this number increases drastically for $\sigma > \sigma_c$ [Fig. 3(c)] after showing a similar behavior (regime) with Fig. 3(b). It is noteworthy that the velocity and stacking fault width of dislocation lines [see also Fig. 5(a) below] were reported just for the first regime. At $\sigma > \sigma_c$, the roughness was averaged from five configurations of dislocation lines at different times. Due to the high fluctuation of dislocation lines in four stronger alloys and to compare
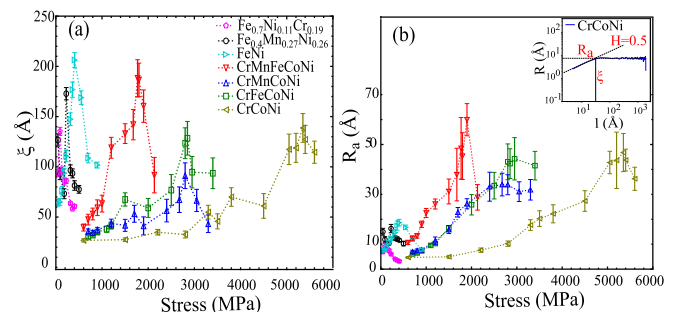

FIG. 4. (a) Mean value of correlation length (ξ) and (b) saturation roughness (R_a) of two partial dislocations which dissociated from an edge dislocation in different HEAs as a function of applied shear stress where the value $H = 0.5$ is fixed.
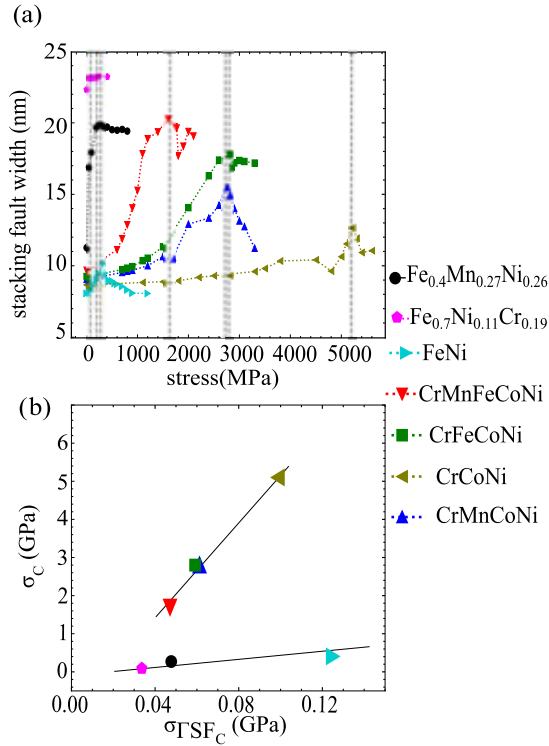
FIG. 5. (a) Stacking fault width between two partial dislocations dissociated from an edge dislocation as a function of applied stress for several HEAs. The vertical dash lines mark the depinning stress for each alloy. (b) Stacking fault stress at depinning stress ($\sigma_{\Gamma SF_c}$) versus σ_c for several HEAs.

the roughness with the same criteria, the correlation length was calculated by considering $H = 0.5$ (see Fig. 4). Figure 4 shows the correlation length (ξ) and saturation roughness (R_a) as a function of stress, although a large correlation length for the three softer materials was observed, with R_a at depinning for four stronger alloys being much larger than the three softer.

Figure 5(a) shows the stacking fault width (W_{SF}) between two partial dislocation lines for each alloy as a function of stress. For W_{SF}, we calculate the average location of each partial dislocation line in the glide direction and then subtract the two. We find that the stacking fault width (W_{SF_c}) is maximum at the depinning stress point σ_c (cf. Ref. [12]). Similarly, a stacking fault stress at the depinning stress ($\sigma_{\Gamma SF_c}$) is calculated [12] from

$$\sigma_{\Gamma SF_c} = \frac{1}{8\pi}\left(\frac{2+\nu}{1-\nu}\right)\left(\frac{\mu_{111/110}b_p}{W_{SF_c}}\right), \quad (1)$$

where b_p, $\mu_{111/110}$, and ν are Burgers vector of each partial dislocation, shear modulus, and Poisson ratio, respectively. $\sigma_{\Gamma SF_c}$ versus σ_c are shown in Fig. 5(b). We see a good correlation between $\sigma_{\Gamma SF_c}$ and σ_c for both types of behavior of the yield stress, separately 5(b) (see the lines to guide the eye). Thus the depinning stress is more sensitive to stacking fault stress for four stronger alloys with a bigger slope. Figure 5(b) [see also hardening factor in Fig. 6(a) below] illustrates again the complex role of dislocation roughness and stacking fault width on the value of the depinning stress. By comparing
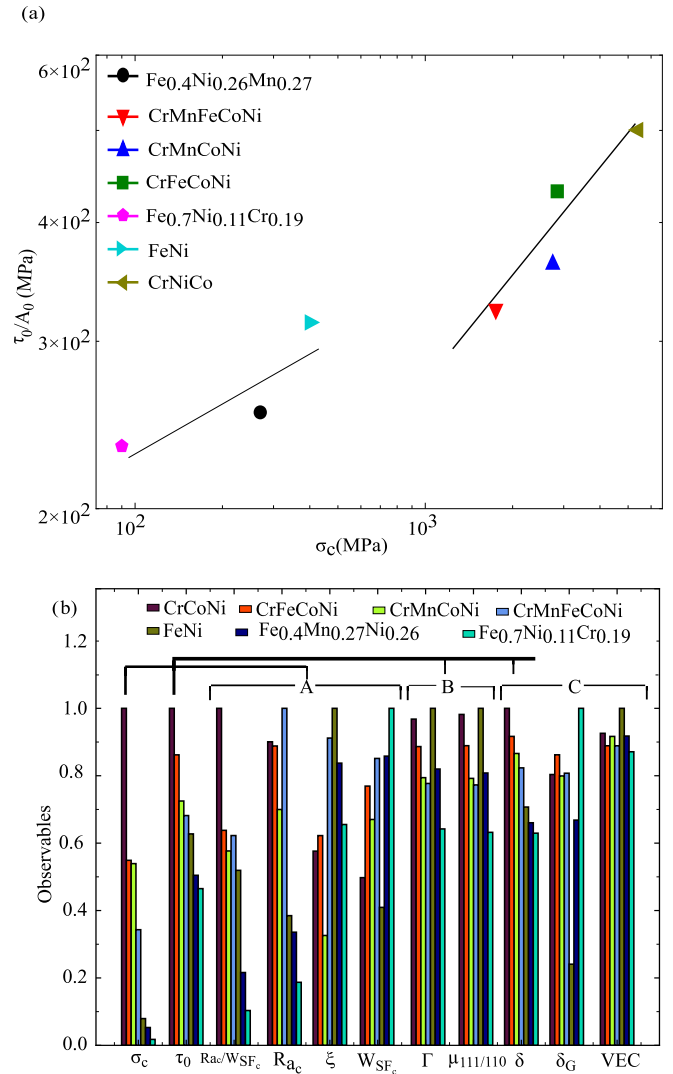

FIG. 6. (a) σ_c versus τ_0/A_0 [Eq. (2)]. (b) σ_c (this study), τ_0 (Varvenne's model), and their related descriptors. Descriptors A [i.e., saturation roughness at depinning stress (R_{a_c}), stacking fault width at depinning stress (W_{SF_c}), hardening factor (R_{a_c}/W_{SF_c}), and correlation length (ξ)] and descriptors B [i.e., line tension (Γ) and shear modulus ($\mu_{111/110}$)] were calculated based on MD simulations, while descriptors C [i.e., atomic misfit (δ), shear modulus misfit (δ_G), and valence electron concentration (VEC)] were calculated based on Refs. [38–40]. All data were normalized for each quantity for the different alloys.

CrCoNi and FeNi in Fig. 5(b), we observe that both have relatively large $\sigma_{\Gamma SF_c}$, but a big difference in respective depinning stresses. This is related to the larger dislocation roughness at depinning for CrCoNi in comparison to FeNi.

In commonly adopted models of solid solution strengthening, the dissociation, in face-centered-cubic (fcc) materials, of an edge dislocation into two partials, during loading, are minimally considered; while, in most cases, the effects are naturally expected to be minimal, they are significant in the case where the roughness of dislocation lines is comparable with the stacking fault width. In particular, it is worth noticing that a solid solution strengthening model for equiatomic alloys [1–4] represents a relationship between the yield stress

at 0 K τ_0, and only the atom size mismatch (δ) [1,2], as

$$\tau_0 \sim \left(\frac{1}{\Gamma}\right)^{\frac{1}{3}} \left(\mu \frac{1+\nu}{1-\nu}\right)^{\frac{4}{3}} (\delta)^{\frac{4}{3}}, \qquad (2)$$

where Γ is line tension. Our results have been developed on the phenomenological basis of Eq. (2) and may be considered in relative agreement. Nevertheless, our results make a further step in the investigation of complex, mutual elastic interactions of rough dislocation partials, when their mutual average distance W_{SF_c} is comparable to the partials' roughness R_{a_c}. While Eq. (2) includes minimal effects of mutually parallel partial dislocations at stacking faults [8], we show that there is a nontrivial interplay of very strong pinning disorder (large R_{a_c}) and relatively small W_{SF_c}. To realize which quantities affect depinning stress, correlation between depinning stress and its descriptors [i.e., saturation roughness at depinning stress (R_{a_c}), stacking fault width at depinning stress (W_{SF_c}), hardening factor (R_{a_c}/W_{SF_c}), and correlation length (ξ)], Varvenne's model yield stress at 0 K and its descriptors [i.e., line tension (Γ) and shear modulus ($\mu_{111/110}$)], misfit parameters and valence electron concentration (VEC) is shown in Fig. 6(b) for all SSAs when the values are normalized. A good correlation between the depinning stress and model predictions for the yield stress is observed for three alloys with the lowest yield stress [Fig. 6(b)], whereas the scaling for the four stronger alloys is different [see Fig. 6(a) with a line to guide the eye].

Figure 6(b) represents the strong correlation between depinning stress and δ, and the ratio of R_{a_c}/W_{SF_c}. The last correlations represent a hardening factor which can explain strengthening based on stacking fault width and element-based chemical disorder. The stronger alloys at depinning stress have high roughness as well as low stacking fault width, indicating that in the four stronger alloys the difference between misfit parameters (misfit shear modulus and misfit atomic size) in the fcc and hcp phase can play an important role where the lower stacking fault width (less number of hcp atoms) leads to a higher strength.

In summary, this study investigated the geometry of edge dislocations and their mobility under the application of external stress for seven random fcc SSAs. At the top four stronger alloys, due to the fact that stacking fault widths are very small, the mutual elastic interactions of the corresponding partials at $\sigma \simeq \sigma_c$ are really high and lead to exceptional strength through an interplay of strong-disorder depinning of two closely spaced and spatially correlated elastic lines. Even though elastic depinning theories [13] have not yet investigated this particular regime, we provided extensive and consistent evidence for the existence of this regime, dominated by roughness-induced strong elastic interactions at the stacking fault that may significantly influence hardening in these materials.

[1] C. Varvenne, A. Luque, and W. A. Curtin, Theory of strengthening in fcc high entropy alloys, Acta Mater. **118**, 164 (2016).

[2] W. G. Noehring and W. Curtin, Correlation of microdistortions with misfit volumes in high entropy alloys, Scr. Mater. **168**, 119 (2019).

[3] B. Gludovatz, A. Hohenwarter, D. Catoor, E. H. Chang, E. P. George, and R. O. Ritchie, A fracture-resistant high-entropy alloy for cryogenic applications, Science **345**, 1153 (2014).

[4] Z. Wu, H. Bei, G. M. Pharr, and E. P. George, Temperature dependence of the mechanical properties of equiatomic solid solution alloys with face-centered cubic crystal structures, Acta Mater. **81**, 428 (2014).

[5] E. P. George, W. Curtin, and C. C. Tasan, High entropy alloys: A focused review of mechanical properties and deformation mechanisms, Acta Mater. **188**, 435 (2020).

[6] R. L. Fleischer, Substitutional solution hardening, Acta Metall. **11**, 203 (1963).

[7] R. Labusch, A statistical theory of solid solution hardening, Phys. Status Solidi B **41**, 659 (1970).

[8] C. Varvenne, A. Luque, W. G. Nöhring, and W. A. Curtin, Average-atom interatomic potential for random alloys, Phys. Rev. B **93**, 104201 (2016).

[9] T. Z. Khan, T. Kirk, G. Vazquez, P. Singh, A. Smirnov, D. D. Johnson, K. Youssef, and R. Arróyave, Towards stacking fault energy engineering in fcc high entropy alloys, Acta Mater. **224**, 117472 (2022).

[10] Y. Zeng, X. Cai, and M. Koslowski, Effects of the stacking fault energy fluctuations on the strengthening of alloys, Acta Mater. **164**, 1 (2019).

[11] D. Molnar, X. Sun, S. Lu, W. Li, G. Engberg, and L. Vitos, Effect of temperature on the stacking fault energy and deformation behaviour in 316l austenitic stainless steel, Mater. Sci. Eng., A **759**, 490 (2019).

[12] A. Vaid, D. Wei, E. Bitzek, S. Nasiri, and M. Zaiser, Pinning of extended dislocations in atomically disordered crystals, arXiv:2110.12507.

[13] D. S. Fisher, Collective transport in random media: from superconductors to earthquakes, Phys. Rep. **301**, 113 (1998).

[14] S. Papanikolaou, Y. Cui, and N. Ghoniem, Avalanches and plastic flow in crystal plasticity: An overview, Modell. Simul. Mater. Sci. Eng. **26**, 013001 (2017).

[15] S. Zapperi and M. Zaiser, Depinning of a dislocation: the influence of long-range interactions, Mater. Sci. Eng., A **309**, 348 (2001).

[16] J.-H. Zhai and M. Zaiser, Properties of dislocation lines in crystals with strong atomic-scale disorder, Mater. Sci. Eng., A **740**, 285 (2019).

[17] G. Péterffy, P. D. Ispánovity, M. E. Foster, X. Zhou, and R. B. Sills, Length scales and scale-free dynamics of dislocations in dense solid solutions, Mater. Theory **4**, 1 (2020).

[18] S. Patinet, D. Bonamy, and L. Proville, Atomic-scale avalanche along a dislocation in a random alloy, Phys. Rev. B **84**, 174101 (2011).

[19] R. Asaro and V. Lubarda, *Mechanics of Solids and Materials* (Cambridge University Press, Cambridge, UK, 2006).

[20] A. P. Thompson, H. M. Aktulga, R. Berger, D. S. Bolintineanu, W. M. Brown, P. S. Crozier, P. J. in 't Veld, A. Kohlmeyer, S. G. Moore, T. D. Nguyen *et al.*, LAMMPS - A flexible simulation tool for particle-based materials modeling at the atomic, meso, and continuum scales, Comput. Phys. Commun. **271**, 108171 (2022).

[21] Y. Shang, J. Brechtl, C. Psitidda, and P. K. Liaw, Mechanical behavior of high-entropy alloys: A review, High-Entropy Materials: Theory, Experiments, and Applications, 435 (2021).

[22] R. Zhang, S. Zhao, J. Ding, Y. Chong, T. Jia, C. Ophus, M. Asta, R. O. Ritchie, and A. M. Minor, Short-range order and its impact on the CrCoNi medium-entropy alloy, Nature (London) **581**, 283 (2020).

[23] Q.-J. Li, H. Sheng, and E. Ma, Strengthening in multi-principal element alloys with local-chemical-order roughened dislocation pathways, Nat. Commun. **10**, 3563 (2019).

[24] M. Yao, K. G. Pradeep, C. C. Tasan, and D. Raabe, A novel, single phase, non-equiatomic FeMnNiCoCr high-entropy alloy with exceptional phase stability and tensile ductility, Scr. Mater. **72**, 5 (2014).

[25] Z. Li and D. Raabe, Strong and ductile non-equiatomic high-entropy alloys: Design, processing, microstructure, and mechanical properties, JOM **69**, 2099 (2017).

[26] S. Plimpton, Fast parallel algorithms for short-range molecular dynamics, J. Comput. Phys. **117**, 1 (1995).

[27] W.-M. Choi, Y. H. Jo, S. S. Sohn, S. Lee, and B.-J. Lee, Understanding the physical metallurgy of the CoCrFeMnNi high-entropy alloy: an atomistic simulation study, npj Comput. Mater. **4**, 1 (2018).

[28] S. Zhao, Y. N. Osetsky, and Y. Zhang, Atomic-scale dynamics of edge dislocations in Ni and concentrated solid solution NiFe alloys, J. Alloys Compd. **701**, 1003 (2017).

[29] Y. N. Osetsky and D. J. Bacon, An atomic-level model for studying the dynamics of edge dislocations in metals, Modell. Simul. Mater. Sci. Eng. **11**, 427 (2003).

[30] H. J. Berendsen, J. v. Postma, W. F. van Gunsteren, A. DiNola, and J. R. Haak, Molecular dynamics with coupling to an external bath, J. Chem. Phys. **81**, 3684 (1984).

[31] A. Stukowski, V. V. Bulatov, and A. Arsenlis, Automated identification and indexing of dislocations in crystal interfaces, Modell. Simul. Mater. Sci. Eng. **20**, 085007 (2012).

[32] A. Stukowski, Visualization and analysis of atomistic simulation data with ovito–the open visualization tool, Modell. Simul. Mater. Sci. Eng. **18**, 015012 (2009).

[33] A. Mughal, L. Laurson, G. Durin, and S. Zapperi, Effect of dipolar interactions for domain wall dynamics in magnetic thin films, IEEE Trans. Magn. **46**, 228 (2010).

[34] F. Bohn, M. A. Corrêa, M. Carara, S. Papanikolaou, G. Durin, and R. L. Sommer, Statistical properties of Barkhausen noise in amorphous ferromagnetic films, Phys. Rev. E **90**, 032821 (2014).

[35] L. Laurson, G. Durin, and S. Zapperi, Universality classes and crossover scaling of Barkhausen noise in thin films, Phys. Rev. B **89**, 104402 (2014).

[36] P.-A. Geslin and D. Rodney, Thermal fluctuations of dislocations reveal the interplay between their core energy and long-range elasticity, Phys. Rev. B **98**, 174115 (2018).

[37] A. Skaugen and L. Laurson, Depinning Exponents of Thin Film Domain Walls Depend on Disorder Strength, Phys. Rev. Lett. **128**, 097202 (2022).

[38] C. Kittel, P. McEuen, and P. McEuen, *Introduction to Solid State Physics* (Wiley, New York, 1996), Vol. 8.

[39] W. Martienssen and H. Warlimont, *Springer Handbook of Condensed Matter and Materials Data* (Springer Science & Business Media, New York, 2006).

[40] S. Guo, C. Ng, J. Lu, and C. Liu, Effect of valence electron concentration on stability of fcc or bcc phase in high entropy alloys, J. Appl. Phys. **109**, 103505 (2011).